Renewable Energy 75 (2015) 123–134

Contents lists available at ScienceDirect

Renewable Energy

journal homepage: www.elsevier.com/locate/renene

An optimization-based approach to scheduling residential battery storage with solar PV: Assessing customer benefit

Elizabeth L. Ratnam*, Steven R. Weller [1], Christopher M. Kellett [1]

The University of Newcastle, School of Electrical Engineering and Computer Science, University Drive, Callaghan, NSW 2308, Australia

ARTICLE INFO

Article history:
Received 31 January 2014
Accepted 5 September 2014
Available online 11 October 2014

Keywords:
Photovoltaics
Battery scheduling
Feed-in tariffs
Time-of-use pricing
Peak-load reduction

ABSTRACT

Several studies have suggested that battery storage co-located with solar photovoltaics (PV) benefits electricity distributors in maintaining system voltages within acceptable limits. However, without careful coordination, these potential benefits might not be realized. In this paper we propose an optimization-based algorithm for the scheduling of residential battery storage co-located with solar PV, in the context of PV incentives such as feed-in tariffs. Our objective is to maximize the daily operational savings that accrue to customers, while penalizing large voltage swings stemming from reverse power flow and peak load. To achieve this objective we present a quadratic program (QP)-based algorithm. To complete our assessment of the customer benefit, the QP-based scheduling algorithm is applied to measured load and generation data from 145 residential customers located in an Australian distribution network. The results of this case study confirm the QP-based scheduling algorithm significantly penalizes reverse power flow and peak loads corresponding to peak time-of-use billing. In the context of feed-in tariffs, the majority of customers exhibited operational savings when QP energy-shifting.

1. Introduction

Climate change, energy security, and limited fossil fuel resources are drivers for the integration of renewable energy sources such as solar into the modern power grid. Significant challenges in converting the abundant solar resource into reliable, high-quality electricity include variability of solar irradiance on both daily and seasonal timescales in addition to intermittency arising from moving cloud cover on timescales of much shorter duration [1,2].

Despite these challenges, governments around the world have in recent years encouraged grid-integrated residential-scale (rooftop) solar photovoltaic (PV) generation through financial incentives such as feed-in-tariffs (FiTs) paid directly to customers [3–5]. These financial incentives in conjunction with a sharp drop in the capital cost of small-scale PV, and increasing electricity prices, have led to the dramatic uptake of residential PV in some countries [6,7]. For example, in Germany PV plant installations exceed 1.2 million, and as of September 2012, peak PV capacity reached 31 GW with about 70% of this 31 GW being connected to the low voltage grid [6].

An adverse consequence of such significant PV penetration in the low voltage electricity distribution network is voltage rise leading to reverse power flow. Voltage rise is particularly pronounced when large numbers of rooftop PV generators are connected in close proximity to each other [8–14]. A further adverse consequence of significant PV penetration is voltage dip. This occurs, for example, when passing cloud cover results in a significant drop in rooftop PV generation [10–12,15]. If these voltage deviations fall outside power quality standards, either the utility covers the direct cost of mitigation or the burden of voltage regulation falls to the PV producer [2,6,8,13,14].

There are two common approaches to managing voltage rise in the low voltage grid. The first is to augment the distribution grid by increasing conductor size and/or upgrading transformers to lower network impedances [6,9,16]. The second is to constrain PV generation at times of low electricity consumption in order to preserve compliance of allowable voltage deviations [13,17,18]. Neither approach is optimal for increased PV penetration as network augmentation adds to the overall PV grid integration costs [9] whereas spilling PV generation leads to lost revenue for the producer.

* Corresponding author. Tel.: +61 2 492 16026; fax: +61 2 492 16993.
E-mail addresses: elizabeth.ratnam@ieee.org (E.L. Ratnam), Steven.Weller@newcastle.edu.au (S.R. Weller), Chris.Kellett@newcastle.edu.au (C.M. Kellett).
[1] Tel.: +61 2 492 16026; fax: +61 2 492 16993.

http://dx.doi.org/10.1016/j.renene.2014.09.008
0960-1481/

Alternative approaches to managing PV generation in the low voltage grid are facilitated through Advanced Metering Infrastructure (AMI) [19–23]. When two way communication is enabled between the utility and customer via AMI, opportunities exist for more advanced demand-side management initiatives that include direct [20,24–28], and price-responsive [21–23,29,30] load control. For example, the utility can enact price-responsive load control by broadcasting a day-ahead time-varying electricity tariff to the AMI. To maintain an existing energy usage level, the customer may choose to schedule battery storage in response to the time-varying electricity tariff or pay a higher energy bill. However without careful coordination of the residential battery schedules, network load curve smoothing via demand-side management initiatives may not be realized [26,31,32].

Several authors have investigated energy-time shifting through battery storage with a focus on minimizing residential energy bills and reducing network peak demand [33–37], leading to battery schedules that either assist or exacerbate non-compliant voltage deviations associated with solar PV. The reduction of network peak demand is incorporated into an optimization problem in Ref. [34], where the objective function includes financial incentives for residents to deliver energy to the grid when the purchase cost of electricity is high. Hence, when interconnected customers in close proximity implement the objective function in Ref. [34], large voltage swings associated with reverse power flow potentially arise due to the battery scheduling. The reduction of network peak demand is also incorporated into a linear program in Ref. [33], where the energy flowing from the point of common coupling (PCC) to the customer is minimized when residential load exceeds residential PV production. Otherwise the battery is scheduled in Ref. [33] to charge during the off-peak pricing period, and discharge during the peak pricing period, with no penalty on increased reverse power flow, potentially exacerbating voltage rise. In contrast, the reduction of network peak demand and the mitigation of undesirable reverse power flow, i.e., load curve smoothing, is incorporated into the optimization problems in Refs. [35–37]. The optimization problem in Ref. [35] achieves load curve smoothing by omitting financial incentives encouraging solar PV uptake (e.g., feed in tariffs or net metering) in the objective function. The optimization problem in Ref. [36] also achieves load curve smoothing by removing incentives for reverse power flow associated with battery scheduling, while permitting incentives encouraging solar PV uptake. Another method for reducing network peak demand while potentially abating reverse power flow is incorporated into the optimization problem in Ref. [37], where a sophisticated dynamic pricing environment provides additional incentives for customers to smooth their day-ahead energy consumption.

Our objective in this paper is similar to [36] in one respect, we seek to maximize residential PV generation co-located with battery storage so that there is a financial benefit to the resident whilst simultaneously alleviating the utility burden associated with peak demand and reverse power flow. Our approach achieves this objective for a range of financial incentives offered for solar PV uptake, such as feed-in tariffs [3–5,36] and net metering [34,38,39], in addition to other more sophisticated dynamic day-ahead pricing rates [23,29,37]. We assume peak billing rates coincide with generation shortages or peak grid demand and look to minimize energy flow from the grid to the customer during these events, while additionally reducing reverse power flow.

Implicit in our approach is the expectation that residential customers have installed Home Energy Management (HEM) systems that: (1) forecast the day-ahead residential load and solar PV generation, (2) coordinate with the AMI to receive day-ahead prices for energy delivered to and from the grid, including any additional PV incentives, (3) run optimization-based algorithms daily, and (4) schedule battery storage in the day-ahead. In this paper we assume the day-ahead forecast of load and generation from the HEM system are known and perfect, and we focus on the formulation of an optimization-based algorithm that provides the day-ahead battery schedule. We also assume the customers' HEM system is fully automated and employs a wireless communication architecture, similar to the description in Ref. [27]. Furthermore, we expect global investment and government mandates will drive both technology improvements and economies of scale for battery storage as has happened with solar PV [40–43]. Therefore our focus is on the operational savings that accrue to a resident when the HEM schedules a battery, and we exclude the capital costs of purchasing a battery from our consideration.

In this paper we consider the quadratic program (QP)-based minimization of the energy supplied by, or to, the grid in a residential PV system with co-located battery storage, first presented in Ref. [44]. Our objective is to smooth network load curves while providing incentives to customers to energy time-shift. In the present paper we remove a bias in the QP-based algorithm in Ref. [44] by including an additional battery constraint related to the state of charge, and with a modification to the greedy-search heuristic that selects the key design parameters in this QP we reduce computational time. Furthermore, we apply the improved QP-based scheduling algorithm to measured load and generation data from 145 Australian residential customers, and investigate the financial savings that accrue to customers. In the present paper, the financial benefit associated with the daily battery charge/discharge schedule is our primary focus in the context of financial incentives offered for solar PV generation such as feed-in tariffs, rather than the utility benefit of load curve smoothing.

This paper is organized as follows. In Section 2 we introduce the optimization-based approach for scheduling battery storage in a residential PV system, and include a motivating example. To assess the customer benefit, we introduce a framework in Section 3 that incorporates different demand-side management approaches for price-response load control, which integrates applicable incentives for PV generation. With this framework we define the daily energy bill for a single customer with and without battery storage. In Section 4 we describe the operations savings associated with battery scheduling, and in Section 5 we present an algorithm for selecting a key design parameter in the QP described in Section 2. In Section 6 we implement the QP-based algorithm given real-world data from 145 residential customers located in an Australian distribution network in the context of feed-in tariffs, and investigate the customer benefit to changes in different elements within the QP (e.g., battery size).

1.1. Notation

Let $\mathbb{R}^s$ denote s-dimensional vectors of real numbers and $\mathbb{R}^s_{\geq 0}$ s-dimensional vectors with all non-negative components where, as usual, $\mathbb{R}^1 = \mathbb{R}$. $\mathbf{I}$ denotes the s-by-s identity matrix and $\mathbb{1} \in \mathbb{R}^s_{\geq 0}$ denotes the all-1 s column vector of length s. $\mathbf{0}$ denotes an all-zero matrix, or an all-zero column vector, where the context will make clear the dimension intended, and $\mathbf{T}=[t_{ij}]$ denotes the s-by-s matrix satisfying $t_{ij}=1$ for $i \geq j$ and $t_{ij}=0$ elsewhere.

2. Problem formulation

2.1. Definitions and constraints

Fig. 1 illustrates the topology of the system under consideration, including a set of meters $\mathcal{M} = \{M_1, M_2, M_3\}$ installed for the purpose of billing and compensation. For each $k \in \{1, \ldots, s\}$, meter M_1 measures the average PV generation g_k (in kW), meter M_2 measures

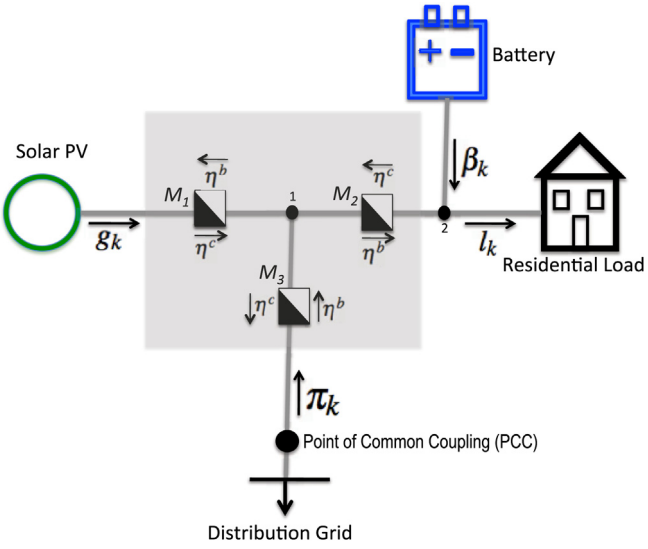

Fig. 1. Residential system illustrating the direction of positive power flows and financial incentives to energy time-shift. Arrows associated with g_k, l_k, β_k and π_k illustrate the assumed direction of positive power flow. Financial incentives for each meter M_1, M_2 and M_3 are represented by vectors η^b and η^c (in \$/kWh), in which arrows illustrate the direction of power flow relevant for η^b and η^c.

the average power from node 1 to node 2 ($l_k-\beta_k$ in kW), and meter M_3 measures the average power π_k (in kW) supplied by (or to) the grid. Meters M_2 and M_3 may be bi-directional, whereas meter M_1 needs only be unidirectional since PV generation satisfies $g_k\geq 0$ for all k. Also shown in Fig. 1 are vectors η^b and η^c, which represent financial incentives for billing and compensation respectively, defined in Section 3.2.

The power flows indicated in Fig. 1 are represented by vectors of length s, where s is the number of time intervals of length Δ, and $T=s\Delta$ (in hours) is the time window of interest. In this paper we generally consider T=24 h, $\Delta = 1/2$ hour (30 min), which implies s=48. Other choices are certainly possible, subject only to commensurability of T, Δ and s.

We represent the average power delivered to the residential load (in kW) over the period $((k-1)\Delta, k\Delta)$ by l_k for all $k\in\{1,\ldots,s\}$, and define the *load profile* over $[0,T]$ as $l := [l_1,\ldots,l_s]^T \in \mathbb{R}^s_{\geq 0}$. Likewise we represent the average PV generation (kW) over the period $((k-1)\Delta,k\Delta)$ by g_k for all $k\in\{1,\ldots,s\}$, and define the *generation profile* over $[0,T]$ as $g := [g_1,\ldots,g_s]^T \in \mathbb{R}^s_{\geq 0}$. In what follows, we assume the day-ahead forecasts of load and generation profiles are known and perfect.

We represent the average power (in kW) supplied by (or to) the grid over the period $((k-1)\Delta,k\Delta)$ by π_k for all $k\in\{1,\ldots,s\}$ and define the *grid profile* over $[0,T]$ as $\pi := [\pi_1,\ldots,\pi_s]^T \in \mathbb{R}^s$. By convention we represent power flowing from (to) the grid to (from) the energy system by $\pi_k>0$ ($\pi_k<0$).

We represent the average power (kW) delivered from (or to) the battery over the period $((k-1)\Delta,k\Delta)$ by $\beta_k > 0$ (or $\beta_k < 0$), and define the *battery profile* over $[0,T]$ as $\beta := [\beta_1,\ldots,\beta_s]^T \in \mathbb{R}^s$. By convention we represent charging (discharging) of the battery by $\beta_k<0$ ($\beta_k>0$).

From the configuration of the residential energy system in Fig. 1, we observe that the following power balance equation

$$l_k = \pi_k + g_k + \beta_k \quad \text{for all } k\in\{1,\ldots,s\}, \tag{1}$$

must hold.

The inclusion of the battery in Fig. 1 leads to additional constraints, which we now detail. To capture the limited "charging/discharging capacity" of the battery, we constrain β by

$$\underline{B}\mathbb{1} \leq \beta \leq \overline{B}\mathbb{1} \tag{2}$$

where $\underline{B}\in\mathbb{R}_{\leq 0}$ and $\overline{B}\in\mathbb{R}_{\geq 0}$.

Given β, the *state of charge* of the battery (in kWh) at time $k\Delta$ is denoted by χ_k, where

$$\chi_k := \chi_0 - \sum_{j=1}^{k} \beta_j\Delta \quad \text{for all } k\in\{1,\ldots,s\}, \tag{3}$$

and χ_0 denotes the initial state of charge of the battery. We represent the *state of charge profile* by $\chi := [\chi_0,\ldots,\chi_s]^T \in \mathbb{R}^{s+1}$.

If we represent the battery capacity (in kWh) by $C\in\mathbb{R}_{\geq 0}$, it necessarily follows that the state of charge profile is constrained by

$$\mathbf{0} \leq \chi \leq C\begin{bmatrix}1\\ \mathbb{1}\end{bmatrix}. \tag{4}$$

For a fixed initial state of charge satisfying $0\leq\chi_0\leq C$, we define $\underline{\mathbf{C}} := (\chi_0/\Delta)\mathbb{1}$, and $\overline{\mathbf{C}} := (1/\Delta)(C-\chi_0)\mathbb{1}$, and rewrite the battery constraints equations (3) and (4) as

$$-\underline{\mathbf{C}} \leq -\mathbf{T}\beta \leq \overline{\mathbf{C}}. \tag{5}$$

In this paper, we optimize a battery profile over a single day. In order to avoid an energy-shifting bias in these results, we insist that the state of charge of the battery at the end of a day is the same as the state of charge of the battery at the beginning of the day, i.e.,

$$\chi_s = \chi_0, \tag{6}$$

where χ_s is the final state of charge at time $s\Delta$.

Let $A_1 \in \mathbb{R}^{4s\times s}$, and $b_1 \in \mathbb{R}^{4s}$ be defined by

$$A_1 := [\mathbf{I} \quad -\mathbf{I} \quad \mathbf{T} \quad -\mathbf{T}]^T, \quad b_1 := \begin{bmatrix}\overline{B}\mathbb{1}^T & \underline{B}\mathbb{1}^T & \mathbf{C}^T & \overline{\mathbf{C}}^T\end{bmatrix}^T. \tag{7}$$

We now substitute equation (7) into equations (2) and (5), and equation (6) into (3), to succinctly write the battery constraints as

$$A_1\beta \leq b_1, \tag{8}$$

$$\mathbb{1}^T\beta = 0. \tag{9}$$

2.2. Objectives

In what follows, we seek to minimize the impact of the residential energy system on the grid, given a financial incentive to energy time-shift, by minimizing

$$\sum_{k=1}^{s} h_k\pi_k^2, \tag{10}$$

where h_k is a selectable weighting such that $h_k\geq 1$ for all $k\in\{1,\ldots,s\}$.

Specifically, given load and generation profiles l and g, and given battery constraints χ_0, C, and $\overline{B}$, $\underline{B}$ we seek a battery profile β and a grid profile π which minimize the expression in (10), subject to satisfaction of the power balance in equation (1).

The minimization in (10) is subject to both inequality and equality constraints imposed by the battery (8) and (9) and the power balance equation in (1), respectively. Lemma 1 below establishes this constrained minimization as a quadratic program (QP).

Lemma 1. The minimization of expression (10), subject to battery constraints (8) and (9) and the power balance equation (1), can be written as

$$\min_{x\in\mathbb{R}^{2s}} x^T H x \tag{11}$$

such that

$$\overline{A}_1 x \le b_1, \tag{12}$$

$$A_2 x = b_2, \tag{13}$$

where

$$x := \begin{bmatrix}\pi^T & \beta^T\end{bmatrix}^T \in\mathbb{R}^{2s}, \quad H := \begin{bmatrix}\mathbf{H} & \mathbf{0}\\ \mathbf{0} & \mathbf{0}\end{bmatrix} \in\mathbb{R}^{2s\times 2s},$$

$$\mathbf{H} := \mathrm{diag}(h_1,\ldots,h_s) \in\mathbb{R}^{s\times s}, \quad \overline{A}_1 := \begin{bmatrix}\mathbf{0} & A_1\end{bmatrix} \in\mathbb{R}^{4s\times 2s},$$

$$A_2 := \begin{bmatrix}\mathbf{0}^T & \mathbb{1}^T\\ \mathbf{I} & \mathbf{I}\end{bmatrix} \in\mathbb{R}^{(s+1)\times 2s}, \quad b_2 := \begin{bmatrix}0\\ l-g\end{bmatrix} \in\mathbb{R}^{s+1}.$$

Proof. The result follows directly from equations (1), (8) and (9).

The grid profile obtained by solving (11) subject to constraints (12) and (13) is said to be *QP energy-shifted* and we will refer to the process of a customer implementing the daily battery and grid profiles obtained by solving (11) subject to constraints (12) and (13) as QP energy-shifting.

2.3. Example

In this example we consider two battery capacities, C=1 kWh and 10 kWh, to illustrate QP energy-shifting at a residence. For both battery capacities, let $\chi_0 = 0.5\,C$ (initial battery state of charge), and $\overline{B} = -\underline{B} = 1$kW (charge/discharge limits).

Let the load and generation profiles l and g be specified as shown in Fig. 2(a), where the residence load includes a utility controlled heated water cylinder [45].[2] Both load and generation profiles are specified for T=24 h, Δ=30 minutes and $s=T/\Delta$=48. Additionally, we let the weights h_k=1 for all $k\in\{1,\ldots,s\}$.

In Fig. 2(a) we observe the load profile peaks around midnight, consistent with the utility switching on the all-electric-heated water cylinder at the customer premises, and the generation profile peaks around midday. Consequently the peak generation does not align with the peak load at the residence.

Fig. 2(b) illustrates the *base-line* grid profile to which we compare the grid profiles in Fig. 2(c) and (d). The base-line grid profile has no battery to time-shift the grid profile π appearing in (10) (C=0 kWh). Therefore π is calculated directly from the power balance equation in (1) with β_k=0. The grid profiles π illustrated in Fig. 2(c) and (d) arise from the solution of the QP in Lemma 1. Comparing the base-line results in Fig. 2(b) to the grid profile in Fig. 2(c), we observe the 1 kW battery charges (β_k<0) to increase the base-line grid profile (e.g., from −1.26 kW to −0.81 kW between 11.30-Midday), and discharges (β_k>0) to reduce the base-line grid profile (e.g., from 3.69 kW to 2.69 kW between 23.30-Midnight). In Fig. 2(d) we observe further reductions in the magnitude of π, except between 23.30-Midnight, due to the battery discharge constraint of 1 kW.

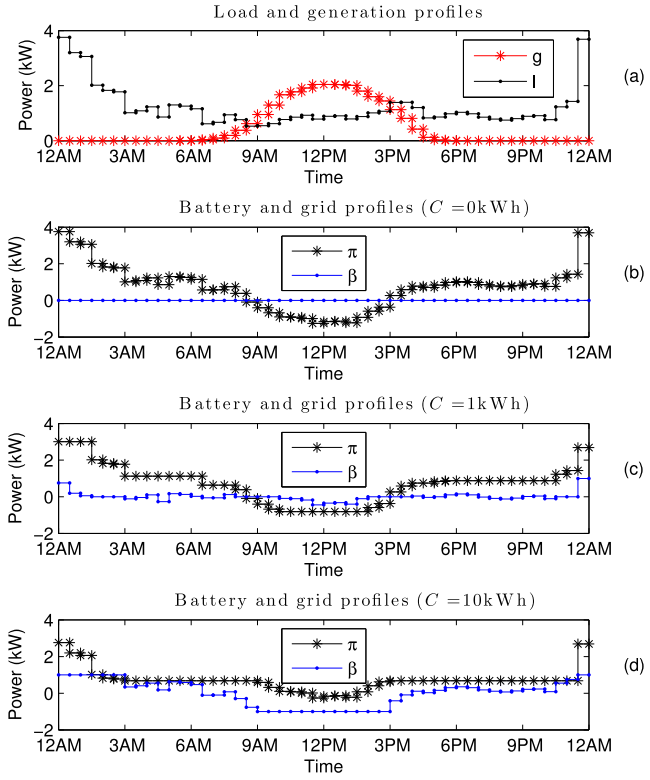

Fig. 2. (a) Load and generation profiles l and g; (b) grid and battery profiles π and β for C = 0 kWh; (c) grid and battery profiles π and β for C = 1 kWh; (d) grid and battery profiles π and β for C = 10 kWh.

This example demonstrates the reductions in magnitude of the grid profile π subject to the battery charge/discharge constraints and capacity C. Hence, QP energy-shifting smooths residential load curves when h_k=1 for all $k\in\{1,\ldots,s\}$. In what follows we design a weighting matrix $\mathbf{H}$ in the QP that reduces residential energy bills, and network peak load corresponding to peak pricing tariffs, while penalizing reverse power flow.

2.4. Extended definition of grid profile

We now extend our definition of *grid usage* over the period $((k-1)\Delta,k\Delta)$ to include explicit reference to the battery capacity C and weights h_k as follows:

$$\pi_k^C(h_k) := l_k - g_k - \beta_k \quad \text{for all } k\in\{1,\ldots,s\}, \tag{14}$$

where l_k, g_k, β_k and h_k remain as previously defined. We consequently denote the *grid profile* over $[0,T]$ by

$$\pi^C(\mathbf{H}) := \left[\pi_1^C(h_1),\ldots,\pi_s^C(h_s)\right]^T \in\mathbb{R}^s. \tag{15}$$

When battery capacity C=0, it follows that

$$\pi_k^0 = l_k - g_k \quad \text{for all } k\in\{1,\ldots,s\}, \tag{16}$$

since the battery charging/discharging capacity β_k=0, $k\in\{1,\ldots,s\}$. The case where C=0 is defined as a *base-line* grid profile against which we compare future grid profiles and is denoted by

[2] In some countries, residents allow the utility to control their all-electric-heated water systems for periods in the day, given a financial incentive. For these customers, the utility switches their water-heating services on during periods of low load, and off during periods of peak-load, in a manner that ensures minimal impact to the network.

$$\pi^0 := \left[\pi_1^0, \ldots, \pi_s^0\right]^T. \quad (17)$$

We note π^0 is not a function of the selectable weights in **H**, as the base-line grid profile is solely a function of load and generation profiles in (16).

Remark 1. The grid profile π obtained from solving the quadratic program in Lemma 1 depends not only on the battery constraints C, $\overline{B}, \underline{B}, \chi_0$, and selected weightings h_k, but also the load and generation profiles l and g, respectively. Consequently π is a function $\pi = \pi(l, g, C, \overline{B}, \underline{B}, \chi_0, \mathbf{H})$. For notational simplicity, however, we will henceforth omit the functional dependence of π on the load/generation profiles and all the battery constraints other than the battery capacity C, preferring instead to simply write $\pi^C(\mathbf{H})$, where no ambiguity arises. This notational convention reflects our primary degrees of design flexibility, namely battery capacity C and the weighting matrix **H**.

3. Billing for a single customer

In this section we define the *energy bill* for a single residential customer for the household PV system depicted in Fig. 1. To reduce the day-ahead energy bill when the customer uses QP energy-shifting (Lemma 1), we require a *financial policy* (in $/kWh) and a battery of capacity C. Since the *financial policy* requires meters in certain locations, with particular modes of operation, we also define the *metering topology* in Section 3.1.

3.1. Metering topology

To formulate the energy bill for a single residential customer, we require the measured power flows from the residential energy system in Fig. 1. The *metering topology* defines how the power flows are to be measured. To formalize the notion of *metering topology* we define two *metering modes* in terms of the meters $M \in \mathscr{M}$, and provide an example with respect to meter M_2 shown in Fig. 1.

1. *Gross metering mode*: We say that meter M_2 operates in *gross metering mode* if it measures power flow from node 1 to the battery/load node 2, but not power delivered in the reverse direction. That is, meter M_2 measures and records only power flows for which $l_k - \beta_k \geq 0$. In the event $l_k - \beta_k < 0$, the meter records 0 kW. Consequently gross metering mode requires only uni-directional metering.
2. *Net metering mode*: We say that meter M_2 operates in *net metering mode* if it measures power flow in both directions, i.e., from node 1 to the battery/load node 2 ($l_k - \beta_k \geq 0$), as well as power delivered in the reverse direction (i.e., $l_k - \beta_k < 0$). Consequently net metering mode requires bi-directional metering [46].

The metering topology is defined by the mode of operation (gross or net) of each meter $M \in \mathscr{M}$ in Fig. 1. In order to consider gross metering mode, the direction of power flow must also be included.

The metering topologies considered in this paper are defined below, with the direction of positive power flow as per Fig. 1, defined in Section 2.1.

- *Metering topology 1*: M_1 and M_2 operate in gross metering mode. M_3 is not installed. M_1 measures and records the generation profile $g_k \geq 0$ for all k, M_2 measures and records the power flow $l_k - \beta_k \geq 0$ for all k.
- *Metering topology 2*: M_3 operates in net metering mode. M_1 and M_2 are not installed.

3.2. Financial policies

To calculate the energy bill for a single residential customer, we require the measured power flows from the residential energy system in Fig. 1, and the corresponding electricity prices. Our definition of a *financial policy* (in $/kWh) formalizes the electricity prices and includes incentives intended to influence customer energy utilization. Example incentives include *time-of-use* (TOU) pricing, *feed-in-tariffs* and *net metering* [3,46]. Our definition of a financial policy below is sufficiently general to include these incentives in addition to more sophisticated dynamic day-ahead pricing rates [23,29,37].

Our definition of a financial policy requires an *electricity billing profile* and an *electricity compensation profile* over $[0,T]$, for each installed meter in $\mathscr{M}$. The direction of power flow associated with electricity billing/compensation is defined with reference to the direction of positive power flow that is specified at each meter $M \in \mathscr{M}$. We denote *electricity billing* (in $/kWh) at meter $M \in \mathscr{M}$ over the period $((k-1)\Delta, k\Delta)$ by $\eta_k^b(M)$ for all $k \in \{1, \ldots, s\}$, and define the *electricity billing profile* over $[0,T]$ at M as $\eta^b(M) := [\eta_1^b(M), \ldots, \eta_s^b(M)]^T \in \mathbb{R}^s_{\geq 0}$. Likewise we denote the *electricity compensation* (in $/kWh) at meter $M \in \mathscr{M}$ over the period $((k-1)\Delta, k\Delta)$ by $\eta_k^c(M)$ for all $k \in \{1, \ldots, s\}$, and define the *electricity compensation profile* over $[0,T]$ at M as $\eta^c(M) := [\eta_1^c(M), \ldots, \eta_s^c(M)]^T \in \mathbb{R}^s_{\geq 0}$.

In order to implement a financial policy, certain types of meters are required in particular locations. For example a financial policy may require the meter M_1 (in Fig. 1), which records positive power flows from the solar PV to node 1. For this meter the financial policy will specify the electricity billing and compensation profiles $\eta^b(M_1)$, $\eta^c(M_1)$, respectively. If the electricity billing (or compensation) profile at meter M_1 is defined by $\eta_k^b(M_1) = 0$ (or $\eta_k^c(M_1) = 0$) for all $k \in \{1, \ldots, s\}$, then it is sufficient that meter M_1 operates in gross metering mode. In this case the power flow to be measured is in the same direction specified for electricity compensation (or billing).

We now define a *financial policy* over $[0,T]$ by using the day ahead electricity billing and compensation profiles at each installed meter in $\mathscr{M}$. An example financial policy is defined with reference to Fig. 1 for $\mathscr{M} = \{M_1, M_2, M_3\}$. The direction of positive power flow at meter M_1 is defined by g (from the solar PV to node 1) and electricity is compensated in this direction $\eta^c(M_1)$. The direction of positive power flow at meter M_2 is defined by $l - \beta \geq 0$ (from node 1 to node 2) and electricity is billed in this direction $\eta^b(M_2)$. The direction of positive power flow at meter M_3 is defined by π (from the PCC to node 1) and electricity is billed in this direction $\eta^b(M_3)$. For each electricity compensation (or billing) profile $\eta^b(M)$ (or $\eta^c(M)$), there also exists an electricity billing (or compensation) profile $\eta^c(M)$ (or $\eta^b(M)$) for power flowing against the positive direction at meter $M \in \mathscr{M}$.

The financial policies considered in this paper are defined with reference to metering topologies 1 and 2 defined in Section 3.1. The financial policy associated with metering topology 1 includes an electricity compensation profile at meter M_1 (for power flow from the solar PV to node 1), and an electricity billing profile at meter M_1 (for power flows in the reverse direction), represented by $\eta^c(M_1)$ and $\eta^b(M_1)$ respectively; and an electricity compensation profile at meter M_2 (for power flow from node 2 to node 1), and an electricity billing profile at meter M_2 (for power flows from node 1 to node 2), represented by $\eta^c(M_2)$ and $\eta^b(M_2)$ respectively. Furthermore, $\eta_k^b(M_1) = 0$ and $\eta_k^c(M_2) = 0$, for all $k \in \{1, \ldots, s\}$ and hence it is sufficient that meters M_1 and M_2 operate in gross metering mode, as per the definition of metering topology 1.

The financial policy associated with metering topology 2 has an electricity compensation profile at meter M_3 (for power flow from node 1 to PCC) and an electricity billing profile at meter M_3 (for

Table 1
Electricity billing and compensation profiles for metering topologies 1 and 2.

Meter	Metering topology 1		Metering topology 2	
	Billing	Compensation	Billing	Compensation
M_1	$\eta^b(M_1)=\mathbf{0}$	$\eta^c(M_1)$		
M_2	$\eta^b(M_2)$	$\eta^c(M_2)=\mathbf{0}$		
M_3			$\eta^b(M_3)$	$\eta^c(M_3)$

power flow from the PCC to node 1), represented by $\eta^c(M_3)$ and $\eta^b(M_3)$ respectively. Table 1 summarizes the electricity billing and compensation profiles for metering topologies 1 and 2.

To implement a gross feed-in tariff, we observe metering topology 1 is sufficient. To implement a net feed-in tariff, or net metering, we observe metering topology 2 is sufficient.

3.3. Energy bill

To define the energy bill for the residential energy system in Fig. 1, we combine the financial policy (in $/kWh) with the measured power flows defined in Section 2.1. To reduce the energy bill when QP energy-shifting, we seek a weighting matrix $\mathbf{H}$ given a fixed battery capacity C.

In what follows we define the *energy bill* (in $/day) in terms of the respective financial policy associated with metering topologies 1 and 2 (Section 3.2). We assume the day-ahead billing and compensation profiles in the respective financial policies are fixed by the utility or regulatory body and available to the consumer.

In equation (6) we constrained the initial and final states of charge of the battery to be equal. Consequently, we assume the cost associated with charging the battery to χ_0 can be compensated for with the remaining charge at the end of the day χ_s. Therefore, in defining of the energy bill, we ignore the cost associated with charging the battery to an initial state of charge.

To formalize the energy bill associated with metering topology 1, we select the electricity prices that correspond to measured power flows at meters M_1 and M_2. That is, for the financial policy relating to metering topology 1, we define $\sigma_k(M_1)$ and $\sigma_k(M_2)$ as follows:

$$\sigma_k(M_1)=\begin{cases}\eta^c_k(M_1), & \text{if } g_k\geq 0\\ \eta^b_k(M_1), & \text{if } g_k<0,\end{cases} \tag{18}$$

$$\sigma_k(M_2)=\begin{cases}\eta^b_k(M_2), & \text{if } l_k-\beta_k\geq 0\\ \eta^c_k(M_2), & \text{if } l_k-\beta_k<0,\end{cases} \tag{19}$$

and denote $\sigma(M_1):=[\sigma_1(M_1),\ldots,\sigma_s(M_1)]^T\in\mathbb{R}^s_{\geq 0}$ and $\sigma(M_2):=[\sigma_1(M_2),\ldots,\sigma_s(M_2)]^T\in\mathbb{R}^s_{\geq 0}$ over the period $[0,T]$. Recall $\eta^b_k(M_1)=0$ and $\eta^c_k(M_2)=0$, for all $k\in\{1,\ldots,s\}$.

In order to minimize the energy bill associated with metering topology 1, we choose the weighting matrix for a given battery capacity with constraints (8) and (9) known and fixed as

$$\mathbf{H}_1:=\mathbf{H}(\sigma(M_1),\sigma(M_2)). \tag{20}$$

Hence the choice of weighting matrix in the cost function (11) is dependent on the implemented financial policy.

Having fixed $\mathbf{H}_1$ in equation (20), we define the residential energy bill associated with metering topology 1, denoted by $\Sigma^C(\mathbf{H}_1)$ (in $/day) by

$$\Sigma^C(\mathbf{H}_1):=\Delta\Big((l-\beta)^T\sigma(M_2)-g^T\sigma(M_1)\Big). \tag{21}$$

When the battery capacity $C=0$, the energy bill defined in (21) reduces to

$$\Sigma^0:=\Delta\Big(l^T\eta^b(M_2)-g^T\eta^c(M_1)\Big), \tag{22}$$

since the battery charging/discharging capacity $\beta_k=0$ for all $k\in\{1,\ldots,s\}$, rendering the selectable weights in $\mathbf{H}_1$ irrelevant. The case where $C=0$ also serves as a *base-line energy bill*, which we use as a comparison when assessing the financial benefits of battery storage.

Remark 2. The energy bill notation convention $\Sigma^C(\mathbf{H}_1)$ is simplified, and consistent with the suppression of functional dependence described in Remark 1. That is, our notation reflects our primary degrees of design flexibility, the battery capacity C and the weighting matrix.

To formalize the energy bill associated with metering topology 2, we select the electricity prices that correspond to measured power flows at meter M_3. That is, we define $\sigma_k(M_3)$ in terms of the financial policy as

$$\sigma_k(M_3)=\begin{cases}\eta^b_k(M_3), & \text{if } \pi^C_k(h_k)\geq 0\\ \eta^c_k(M_3), & \text{if } \pi^C_k(h_k)<0,\end{cases} \tag{23}$$

and we denote $\sigma(M_3):=[\sigma_1(M_3),\ldots,\sigma_s(M_3)]^T\in\mathbb{R}^s_{\geq 0}$ over the period $[0,T]$. In order to minimize the energy bill associated with metering topology 2, we choose the weighting matrix for a given battery capacity with constraints (2)–(4) known and fixed as

$$\mathbf{H}_2:=\mathbf{H}(\sigma(M_3)). \tag{24}$$

Having fixed $\mathbf{H}_2$ in (24), we define the energy bill associated with the financial policy relating to metering topology 2 by

$$\Sigma^C(\mathbf{H}_2):=\Delta\pi^C(\mathbf{H}_2)^T\sigma(M_3), \tag{25}$$

which reduces to the *base-line energy bill* for $C=0$ given by

$$\Sigma^0:=\Delta(l-g)^T\sigma(M_3), \tag{26}$$

where $\pi^0=l-g$ since the battery charging/discharging capacity satisfies $\beta_k=0$ for all $k\in\{1,\ldots,s\}$.

4. Savings for a single customer

In this section we define the energy savings for the household PV system depicted in Fig. 1. The results in this section allow a single customer to assess the cost-effectiveness of installing a battery of a given size. Recall, this paper focuses on the operational energy savings associated with QP energy-shifting and as such we omit the capital cost of installing a battery.

4.1. Energy savings

To examine the effectiveness of QP energy-shifting for a given size battery, we define the *energy savings* (in $/day). The energy savings are denoted by $\Psi^C(\mathbf{H})$ and defined by

$$\Psi^C(\mathbf{H}):=\Sigma^0-\Sigma^C(\mathbf{H}). \tag{27}$$

We recall from Section 3.3, the energy bill $\Sigma^C(\mathbf{H})$ is defined for a particular financial policy and selection of weights in $\mathbf{H}$, given load and generation profiles l and g, a battery of a given size C, with constraints (2)–(4) known and specified. When $C=0$, Σ^0 denotes the base-line energy bill.

Given unique load and generation profiles for 365 consecutive days and a battery of a given size C, with constraints (2)–(4) known

and specified, their exists a unique energy saving $\Psi^C(\mathbf{H})$ for each of the 365 days. We define the summation of these unique energy savings by $\Theta^C(\mathbf{H})$ in \$/yr and label this summation the *annual savings*. Thus when the annual savings are positive, there exists an operational benefit to QP energy-shifting.

Hence $\Theta^C(\mathbf{H})>0$ implies the installation is operationally cost-effective, $\Theta^C(\mathbf{H})=0$ implies the installation is operationally cost-neutral and $\Theta^C(\mathbf{H})<0$ implies no financial benefit for battery storage for that given year.

4.2. Special case: zero energy savings

Consider the special case where there is a fixed price for electricity (in \$/kWh) at all installed meters in $\mathscr{M}$, irrespective of power flow direction and time of day. Lemma 2 below demonstrates that under these circumstances, there is no financial incentive for a resident to install battery storage. That is, since the battery acts as an energy time-shifter, the lack of differential pricing at any point in time gives no incentive to energy time-shift.

Lemma 2. Fix $\eta>0$ and let the electricity billing and compensation profiles in the financial policy satisfy the following for all $M\in\mathscr{M}$:

$$\eta_j^b = \eta_k^c = \eta \quad \text{for all } j,k\in\{1,\dots,s\}, \tag{28}$$

$$\eta^b = \eta^c = \eta\mathbb{1}. \tag{29}$$

Assume all meters $M\in\mathscr{M}$ are installed such that all power flowing to or from the grid is quantifiable (for example metering topology 1 or 2). Then for all choices of battery capacity C and weighting matrix $\mathbf{H}$, the energy savings are $\Psi^C(\mathbf{H})=0$.

Proof. Consider metering topology 2. Rearranging equation (3) yields

$$\chi_0 - \chi_s = \sum_{k=1}^{s} \beta_k \Delta. \tag{30}$$

Recall from the definition of the time window T, we require Δ to be positive ($\Delta > 0$) and a constant. Combining the definition of Δ with the constraint in equation (6) implies

$$\sum_{k=1}^{s} \beta_k = \beta^T\mathbb{1} = 0. \tag{31}$$

Furthermore, definitions (14) and (15) imply

$$\pi^C(\mathbf{H}_2) = l - g - \beta. \tag{32}$$

Additionally, substituting equations (28) and (29) into equation (23) yields

$$\sigma(M_3) = \eta\mathbb{1}. \tag{33}$$

Therefore, from equation (25) the energy bill is

$$\begin{aligned}\Sigma^C(\mathbf{H}_2) &= \Delta\pi^C(\mathbf{H}_2)^T\sigma(M_3) = \Delta(l-g-\beta)^T\eta\mathbb{1}\\ &= \Delta(l-g)^T\eta\mathbb{1} - \Delta\eta\beta^T\mathbb{1} = \Delta(l-g)^T\sigma(M_3) = \Sigma^0,\end{aligned}$$

where the final equality is defined in equation (26).

The energy savings (27) are then

$$\Psi^C(\mathbf{H}_2) = \Sigma^0 - \Sigma^C(\mathbf{H}_2) = 0. \tag{34}$$

A similar calculation can be performed for other metering topologies, provided the meters in $\mathscr{M}$ are installed such that all power flowing to or from the grid is quantifiable.

5. Heuristic for selecting the weighting matrix

In this paper our objective is to maximize the daily operational savings that accrue to a single customers, while penalizing large voltage swings observed in the distribution network stemming from reverse power flow and peak load. We assume peak electricity billing rates coincide with generation shortages or peak grid demand and look to prioritize the minimization of energy flow from the grid during these events, while penalizing reverse power flow. To achieve our objective, we seek a weighting matrix $\mathbf{H}$ in the QP for a single customer with battery storage in the residential setting shown in Fig. 1. Given perfect day-ahead load and generation forecasts, and battery constraints (8) and (9), the HEM system computes the weighting matrix $\mathbf{H}$ via a heuristic for each day-ahead. We define the heuristic in what follows.

In Section 2.2, the minimization of expression (10) was presented as a constrained quadratic program (Lemma 1), where the weights h_k in $\mathbf{H}$ were selectable. In this section we consider the specification of the matrix $\mathbf{H}$ that maximizes the annual savings, while reducing the impact of the residential system on the grid. In practice, the matrix $\mathbf{H}$ is difficult to obtain, as it depends on a variety of factors including financial policies, metering topologies and daily variations in load and generation profiles. To address this problem we propose a greedy-search heuristic for obtaining a so-called *preferred* $\mathbf{H}$, which is in turn based upon a *base-line* weighting matrix denoted by $\mathbf{H}_0$.

When selecting the weights in the preferred $\mathbf{H}$, our rationale is to increase base-line weights when electricity billing is high and decrease base-line weights when electricity billing is low, and to continue increasing/decreasing so long as the daily residential savings increase. This rational reduces network peak loads without contributing to reverse power flow during the peak pricing period, and increases operational savings that accrue to customers.

The basic idea of the heuristic is to increase each weight h_k in $\mathbf{H}_0$, as long as this increase leads to an increased energy saving in (27). To mitigate against numerical difficulties with the solution of the quadratic program in Lemma 1, we increase weights in $\mathbf{H}_0$ until a maximum allowable value of h_k is reached. To this end, weights in $\mathbf{H}_0$ are scaled by the minimum cost and capped at a maximum value. To cap the weights h_k we introduce the following saturation operation:

$$\text{sat}_1^{\overline{h}}(h_k) := \begin{cases} 1, & \text{if } h_k < 1 \\ h_k, & \text{if } 1 \le h_k \le \overline{h} \\ \overline{h}, & \text{if } h_k > \overline{h}, \end{cases} \tag{35}$$

where the lower bound is 1 in accordance with the definition of h_k in Section 2.2 and $\overline{h} > 1$ is fixed. The constant $\overline{h}$ is chosen to mitigate against numerical difficulties in solving the QP in Lemma 1. In this paper, we set $\overline{h} = 1000$.

To formalize the definition of the base-line weighting matrix, let

$$\tilde{\eta}_k := \sum_{M\in\mathscr{M}} \eta_k^b(M), \quad \forall\ k\in\{1,\dots,s\} \tag{36}$$

$$\eta^\star := \min_{k\in\{1,\dots,s\}} \tilde{\eta}_k, \tag{37}$$

and define the base-line weighting matrix $\mathbf{H}_0$ as

$$\mathbf{H}_0 := \mathrm{diag}\left[\mathbf{H}_0^{(1)}, \ldots, \mathbf{H}_0^{(k)}, \ldots, \mathbf{H}_0^{(s)}\right], \tag{38}$$

where $\mathbf{H}_0^{(k)} := \mathrm{sat}_1^{\overline{h}}(\tilde{\eta}_k/\eta^\star)$

Given $\mathbf{H}_0$, the proposed heuristic requires the function for energy savings $\Psi(\cdot)$ defined in (27). Recall the energy savings function $\Psi(\cdot)$ requires the constraints and solution to the QP in Lemma 1 and the energy bill $\Sigma(\cdot)$ pertaining to a given metering topology and financial policy as defined in Section 3. To simplify the notation, we use $\Psi(\cdot)$ rather than $\Psi^C(\mathbf{H})$ to indicate that the battery capacity C is fixed.

The main loop in the heuristic below (lines 6–19), doubles weights in $\mathbf{H}_0$ progressively, from the largest to the smallest element in $\mathbf{H}_0$. If there exist multiple elements in $\mathbf{H}_0$ with the same magnitude, we double the multiple elements concurrently. The set of live indices $\tilde{s}$ keeps track of the indices in $\mathbf{H}_0$ that are yet to be increased, and $\mathbf{I}^{\tilde{s}}$ denotes an s-by-s matrix in which $\mathbf{I}^{\tilde{s}}_{jj} = 1$ if $j \in \tilde{s}$ and zero otherwise.

6. Application of QP energy-shifting

We analyzed measured load and generation profiles from July 1st 2010 to the 30th of June 2011, for each of 300 randomly selected low voltage customers located in an Australian distribution network, operated by Ausgrid. The Ausgrid distribution network covers 22,275 km^2 and includes load centers in Sydney and regional New South Wales.

The load and generation profiles l and g for each of the 300 customers are defined with T=24 h, Δ=30 minutes, and s=T/Δ=48, for each day in the 365 days.

We eliminated customers with a maximum load or PV generation less than 5 W on any day of the year (l_k<0.005 or g_k<0.005 for all $k \in \{1, \ldots, s\}$), leaving 145 of the original 300 customers. We refer to this set of 145 customers as *the ensemble*.

When QP energy-shifting, the annual savings for each customer in the ensemble are dependent on a variety of factors and we investigate four of the most important factors in what follows. In Section 6.2 we investigate the influence of daily variations in the load and generation profiles on savings for particular customers in the ensemble. In Section 6.3 we compare annual savings for different metering topologies. In Section 6.4 we compare annual savings with and without the preferred $\mathbf{H}$. In Section 6.5 we investigate the influence of battery capacity on annual savings. The computational time when QP energy-shifting (including the time to find the preferred $\mathbf{H}$) on each day for each ensemble member is on average 0.422 s with an Intel i7-2630QM processor.

6.1. Simulation parameters

In the following we use the heuristic to find the $\mathbf{H}$ matrix when QP energy-shifting, except as specified in Section 6.4. To calculate the annual savings for the ensemble when QP energy-shifting, we fix the battery capacity at 10 kWh, except in Section 6.5 where we vary the battery capacity within the range 0 kWh $\leq C \leq$30 kWh. In all cases, the remaining battery constraints (2)–(4) are chosen as

Heuristic: Returns the preferred $\mathbf{H}$ given $\Psi(\cdot)$

Input: l, g, C, $\overline{B}$, $\underline{B}$, χ_0, π^0, $\overline{h}$, $\mathbf{H}_0$, $\mathbf{H} = \mathbf{I}$, $\Psi_0 = \Psi(\mathbf{H}_0)$, $\tilde{s} = \{1, \ldots, s\}$

1 **for** $k \in \{1, \ldots, s\}$ **do**
2 **if** $\pi_k^0 = 0$ **then**
3 $q = \{p \in \{1, \ldots, s\} | \pi_p^0 = 0\}$
4 $\tilde{s} = \tilde{s} \setminus q$
5 $\mathbf{H}_0^{(q)} = 1$
6 **while** $\mathbf{H}_0^{(\tilde{s})} > 1$ **do**
7 $k^\star = \arg\max_{\tilde{s}}(\mathbf{H}_0^{(\tilde{s})})$
8 $J = \{j \in \{1, \ldots, s\} | \mathbf{H}_0^{(j)} = \mathbf{H}_0^{(k^\star)}\}$
9 $\forall j \in J \quad \overline{\mathbf{H}}_0 = \mathrm{diag}\left[\mathbf{H}_0^{(1)}, \ldots, 2\mathbf{H}_0^{(j)}, \ldots, \mathbf{H}_0^{(s)}\right]$
10 $\forall j \in J \quad \overline{\mathbf{H}}_0^{(j)} = \mathrm{sat}_1^{\overline{h}}\left(\overline{\mathbf{H}}_0^{(j)}\right)$
11 $\overline{\Psi}_0 = \Psi(\overline{\mathbf{H}}_0)$
12 **while** $\overline{\Psi}_0 > \Psi_0$ **and** $\overline{\mathbf{H}}_0^{(k^\star)} < \overline{h}$ **do**
13 $\Psi_0 = \Psi(\overline{\mathbf{H}}_0)$
14 $\mathbf{H}_0 = \overline{\mathbf{H}}_0$
15 $\forall j \in J \quad \overline{\mathbf{H}}_0 = \mathrm{diag}\left[\mathbf{H}_0^{(1)}, \ldots, 2\mathbf{H}_0^{(j)}, \ldots, \mathbf{H}_0^{(s)}\right]$
16 $\forall j \in J \quad \overline{\mathbf{H}}_0^{(j)} = \mathrm{sat}_1^{\overline{h}}\left(\overline{\mathbf{H}}_0^{(j)}\right)$
17 $\overline{\Psi}_0 = \Psi(\overline{\mathbf{H}}_0)$
18 $\forall j \in J \quad \mathbf{H} = \mathrm{diag}\left[\overline{\mathbf{H}}_0^{(1)}, \ldots, \overline{\mathbf{H}}_0^{(j)}, \ldots, \overline{\mathbf{H}}_0^{(s)}\right]$
19 $\tilde{s} = \tilde{s} \setminus J$
20 $\mathbf{H} = \mathbf{H} + \mathbf{I}^{\tilde{s}}$

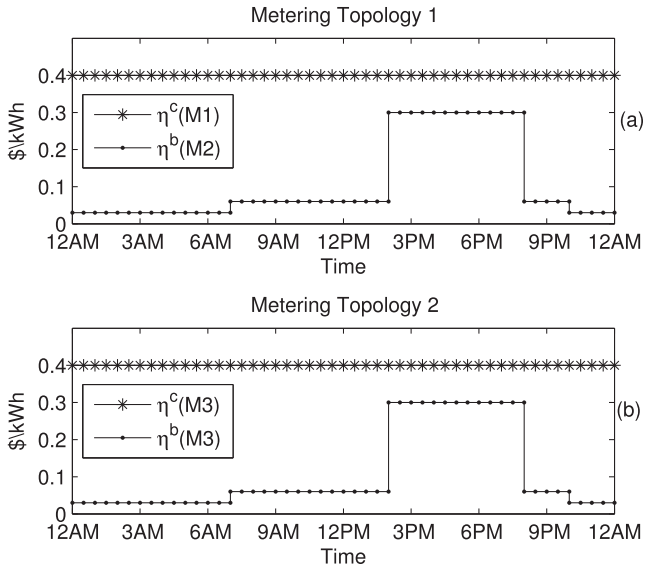

Fig. 3. Non-zero billing and compensation profiles for metering topologies 1 and 2.

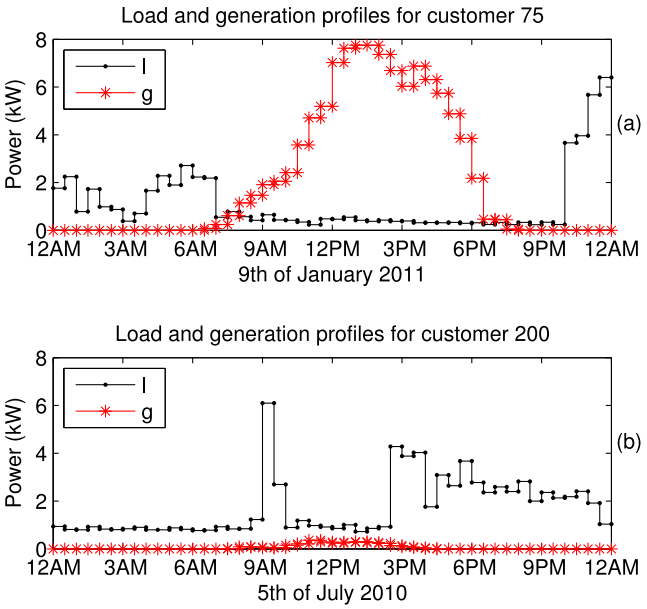

Fig. 4. Representative load and generation profiles for customers 75 and 200.

χ_0=0.5 C, and $\overline{B} = -\underline{B} = 5$kW. We also fix the length-s billing and compensation profiles (each given in \$/kWh) for metering topology 1 as follows:

$$\eta^b(M_1) = \eta^c(M_2) = [0, \ldots, 0]^T,$$

$$\eta^c(M_1) = [0.4, \ldots, 0.4]^T,$$

$$\eta^b(M_2) = \left[\ldots, \eta^b_k, \ldots\right]^T,$$

where $\eta^b_{1-14} = 0.03, \eta^b_{15-28} = 0.06, \eta^b_{29-40} = 0.3, \eta^b_{41-44} = 0.06$, and $\eta^b_{45-48} = 0.03$. The non-zero profiles are shown in Fig. 3(a).

For metering topology 2, the length-s compensation and billing profiles (in \$/kWh) are again fixed and given by

$$\eta^c(M_3) = [0.4, \ldots, 0.4]^T,$$

$$\eta^b(M_3) = \left[\ldots, \eta^b_k, \ldots\right]^T,$$

such that $\eta^b(M_3)$=$\eta^b(M_2)$. The non-zero profiles are shown in Fig. 3(b).

For both metering topologies in Fig. 3 we describe electricity billing from 10pm to 7am at the rate of \$0.03/kWh as an *off-peak pricing period*, electricity billing from 7am to 2pm and again from 8pm to 10 pm at the rate of \$0.06/kWh as a *shoulder pricing period* and electricity billing from 2pm to 8pm at the rate of \$0.30/kWh as a *peak pricing period*.

For metering topology 1 in Fig. 3 we describe electricity compensation $\eta^c(M_1)$ as a gross feed-in tariff. For metering topology 2 in Fig. 3 we describe electricity compensation $\eta^c(M_3)$ as a net feed-in tariff.

6.2. Influence of load and generation profiles

In this section we identify typical load and generation profiles that result in either a positive or negative operational saving when QP energy-shifting under metering topology 1. To do this we compare daily energy savings for two customers in the ensemble. The selected two customers are chosen with significant differences in their respective load and generation profiles (l and g). The two representative customers are denoted Customer 75 and Customer 200.

Fig. 4 illustrates the significant differences in the respective load and generation profiles for customers 75 and 200. In Fig. 4(a) we observe Customer 75 consumed most of its energy during the off-peak pricing period between 10pm and 7am. Meanwhile the solar PV unit delivered energy from 7am to 7:30pm and was in excess of the residential energy demand from 8am to 7:30pm. Consequently, Customer 75 delivered energy to the grid from 8am to 7:30pm on the 9th of January 2011.

In Fig. 4(b) we observe Customer 200 consumed a significant proportion of its energy during the peak pricing period (2pm-8pm) and very little energy during the off-peak pricing period (10pm − 7am). In Fig. 4(b) we also observe the generation profile is less than the load profile for the entire day (g_k<l_k for all $k \in \{1, \ldots, s\}$).

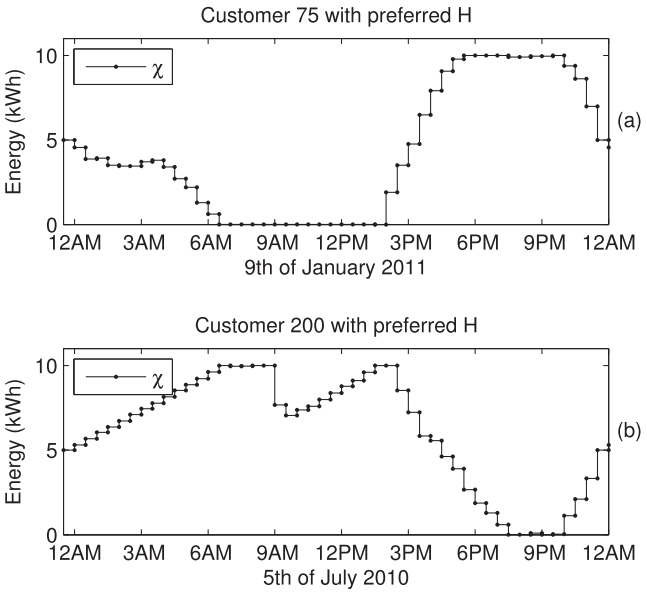

Fig. 5. The battery SOC for customers 75 and 200 when using QP energy-shifting on the 9th of January 2011 and the 5th of July 2010, respectively.

Consequently, there was no energy delivered to the grid by Customer 200 on the 5th of July 2010.

For both customers 75 and 200, given a financial policy associated with metering topology 1 and simulation parameters defined in Section 6.1, we calculate the daily energy savings given a 10 kWh battery. From these daily energy savings we find Customer 75 would have lost $2.68 on the 9th of January 2011 and Customer 200 would have saved $2.70 on the 5th of July 2010 by using QP energy-shifting.

To understand why QP energy-shifting would save Customer 200 $2.70, while costing Customer 75 $2.68, given the load and generation profiles in Fig. 4, we compare the respective battery states of charge. In Fig. 5(a) we observe the battery discharges mostly during the off-peak pricing period when Customer 75 consumed most of its energy and charges during the peak pricing period rather than the shoulder pricing period when PV generation was high and load low due to the weightings imposed via the heuristic. Consequently the cost of charging the battery is not offset by the cost of discharging the battery for Customer 75 on the 9th of January 2011.

In Fig. 5(b) we observe the battery discharges mostly during the peak pricing period when the customer consumed most of its energy and charges during the off-peak pricing period as well as when the solar PV generated energy. Therefore the cost of charging the battery is offset by the cost of discharging the battery for Customer 200 on the 5th of July 2010.

On each day from the 1st of July 2010 to the 30th of June 2011 we calculated the daily energy savings for customers 75 and 200. Fig. 6 illustrates the distribution of these daily savings. In Fig. 6(a) we observe QP energy-shifting results in Customer 75 losing money over the course of a year, even though some days provide savings. This loss of money is attributed to load and generation profiles that caused the battery to charge during peak pricing periods and discharge during off-peak pricing periods, consistent with our observations in Fig. 5(a).

In Fig. 6(b) we observe QP energy-shifting results in Customer 200 saving money over the course of a year. This saving is attributed to load and generation profiles that cause the battery to charge during the off-peak pricing periods and discharge during the peak pricing periods, consistent with our observations in Fig. 5(b).

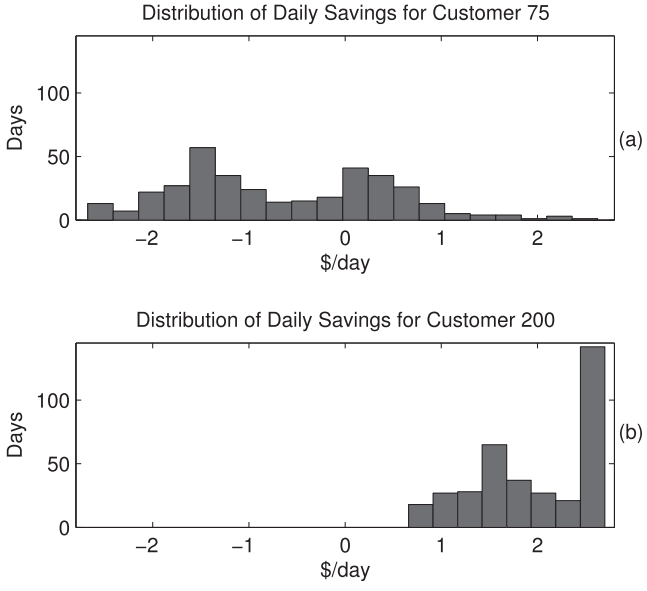

Fig. 6. Distribution of daily saving resulting form QP energy-shifting for customers 75 and 200.

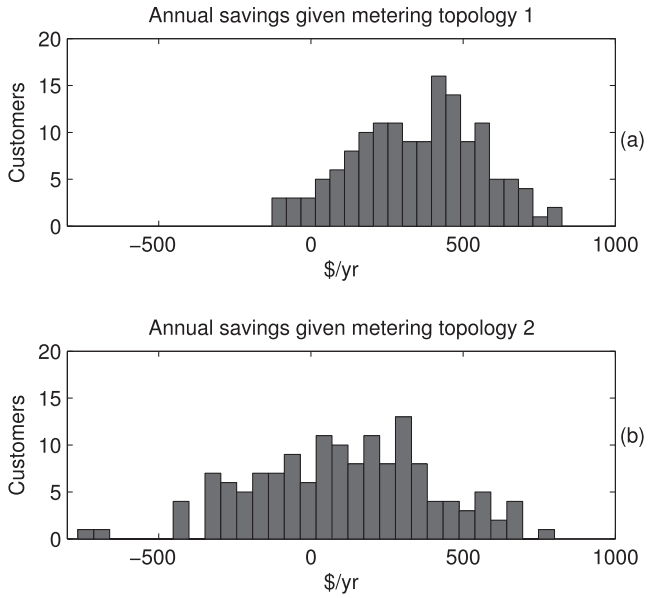

Fig. 7. Annual savings distribution for the ensemble resulting from metering topologies 1 and 2.

Consequently, given metering topology 1, the daily cost of charging a given battery must be offset by the daily cost of discharging a given battery for a customer to reap the benefits of QP energy-shifting. Therefore, given the financial policy associated with metering topology 1 described in Section 6.1, customers that consume most of their energy during the off-peak pricing period and generate more energy then they consume, will not financially benefit from QP energy-shifting. On the other hand, those who consume most of their energy during the peak pricing period and generate less energy then they consume, will financially benefit from QP-energy shifting.

6.3. *Influence of metering topologies*

For each customer in the ensemble, we now calculate and compare the annual savings associated with QP energy-shifting given the financial policy associated with either metering topology 1 or 2 as presented in Section 3.1. For each customer, the annual savings are again calculated for a 10 kWh battery and in all cases, the simulation parameters are as defined in Section 6.1.

Fig. 7 illustrates the distribution of annual savings for all customers in the ensemble under two metering topologies. In Fig. 7(a) we observe metering topology 1 saves the ensemble on average $350/yr, however nine customers lose money, including Customer 75. In Fig. 7(b) we observe metering topology 2 saves the ensemble on average $100/yr, however fifty customers lose money, including Customer 75. Hence some customers do not benefit from QP energy-shifting, irrespective of the metering topology.

We again visit the representative load and generation profiles for Customer 75 in Fig. 4(a) to understand the underlying principles that result in Customer 75 not benefiting from QP energy-shifting, given metering topology 2. In Fig. 4(a) we observed Customer 75 generated energy and delivered most of this energy to the grid and was compensated for this at $0.40/kWh. However if Customer 75 employed QP energy-shifting, the generated energy would instead charge a battery when in excess of the load, leading to a loss in compensation at $0.40/kWh. Given the financial policy relating to

Table 2
Mean Annual Savings for the ensemble.

Battery	Metering topology 1		Metering topology 2	
	$\mathbf{H}_0$	**H**	$\mathbf{H}_0$	**H**
10 kWh	\$266/yr	\$348/yr	\$9/yr	\$90/yr

metering topology 2, it is not possible for this customer to recoup this compensation loss by discharging the battery, as the maximum billing rate is \$0.30/kWh. Therefore, customers that would ordinarily deliver energy to the grid, may not profit from QP energy-shifting when electricity compensation is in excess of electricity billing.

6.4. Influence of the selection of *H*

In this section we verify the heuristic proposed in Section 5. The heuristic finds a matrix **H** that increases the annual savings, with comparison to the base-line **H** (denoted $\mathbf{H}_0$). The results in this section are based on the battery constraints and financial policies as per Section 6.1.

For each customer in the ensemble we calculate the annual savings when QP energy-shifting using both the preferred **H** and $\mathbf{H}_0$ given the financial policies associated with metering topologies 1 and 2. We then average the annual savings of the ensemble and label this average the *mean annual savings* (in \$/yr).

We record the mean annual savings for both the preferred **H** and $\mathbf{H}_0$ in Table 2. From this table we observe the preferred **H** increases mean annual savings when QP energy-shifting, irrespective of the metering topology. Hence the heuristic given in Section 5 successfully increases the mean annual savings for the ensemble, with comparison to $\mathbf{H}_0$.

6.5. Influence of the battery capacity

To assess the influence of battery capacity (in kWh) on residential annual savings when QP energy-shifting we consider again customers 75 and 200 from the ensemble. For these customers we vary the battery capacity (C) given the set of battery capacities (in kWh) C={0,0.1,1,2,4,6,8,10,15,20,30} and plot the results in Fig. 8.

In Fig. 8 we observe that an increase in the battery capacity results in an increase in financial losses for Customer 75. In comparison, an increase in battery capacity results in an increase in annual savings for Customer 200. Furthermore, the increase in annual savings for Customer 200 rapidly approaches an asymptotic value with a 30 kWh battery providing minimal additional savings over a 15 kWh battery. Consequently, not all customers benefit from battery storage and increasing the size of the battery does not necessarily increase the annual savings for a given customer.

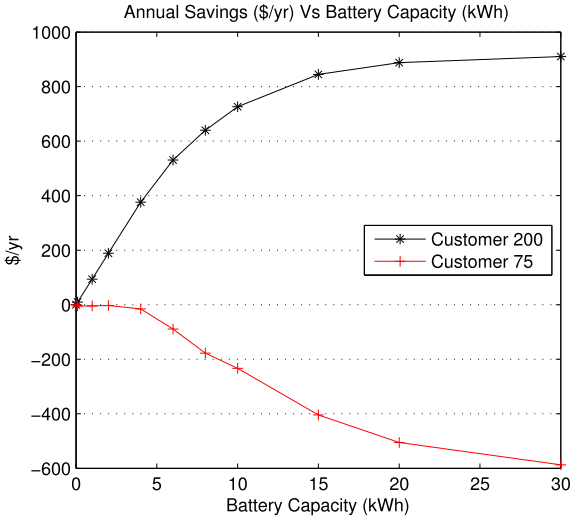

Fig. 8. Comparison of annual savings for customers 200 and 75 with variable battery capacities, under the financial policy pertaining to metering topology 1.

Considering the subset of customers who do financially benefit from QP energy-shifting, if we know the capital cost of installing a battery of a given size, with constraints known and specified, Fig. 8 may be useful in identifying the most cost-effective battery capacity. Furthermore, given the capital cost of installing a battery, we expect there also exists a critical annual saving where increases in battery capacity may no longer be cost-effective.

7. Conclusions

In this paper we have presented a QP-based algorithm for day-ahead scheduling of residential battery storage co-located with solar PV. The QP-based algorithm is formulated to balance two objectives. The first objective is to minimize the impact of the residential system on the grid, by reducing the network peak demand and non-compliant voltage deviations associated with reverse power flow. The second objective is to increase the daily operational savings that accrue to customers, by time-shifting residential load from peak pricing periods to off-peak pricing periods. In particular, we balance the reduction of load during during peak pricing periods with penalties for reverse power flow during the same period so that voltage rise associated with solar PV is not simply time-shifted to the peak pricing periods. Furthermore, our proposed framework allows for a variety of financial incentives and their required metering topologies.

Our QP-based algorithm requires a user-specified weighting matrix, **H**. We have presented a heuristic approach to the specification of **H**. Other approaches are possible, and may provide improved customer benefits.

In the context of feed-in tariffs we assessed the customer benefit of QP energy-shifting by using measured load and generation data from 145 residential customers located in an Australian distribution network. In assessing the potential benefit for each of these customers, we observed that most, but not all, customers see operational savings. Customers who are offered incentives to generate more electricity then they consume, with peak load falling outside the peak and shoulder pricing periods, are included in the category of negative operational savings. Further work is needed to more completely characterize suitable financial policies, metering topologies, and battery size with respect to financial benefits of QP energy-shifting for customers who observed negative operational savings.

Acknowledgments

Elizabeth L. Ratnam acknowledges the financial support of an Australian Postgraduate Award (APA) and a CSIRO – Energy Technology Postgraduate Research Scholarship (Ref: 2011094123).

References

[1] Radchik A, Skryabin I, Maisano J, Novikov A, Gazarian T. Ensuring long term investment for large scale solar power stations: Hedging instruments for green power. Part B Sol Energy 2013;98:167–79.
[2] CSIRO. Solar intermittency: Australia's clean energy challenge. Tech. rep. CSIRO; June 2012.
[3] Del Carpio-Huayllas TE, Ramos DS, Vasquez-Arnez RL. Feed-in and net metering tariffs: An assessment for their application on microgrid systems. In: Proc. 6th IEEE/PES Latin America Conf. and Exposition on Transmission and Distribution (T&D-LA'12), Montevideo, Uruguay; 2012. p. 1–6.

[4] Campoccia A, Dusonchet L, Telaretti E, Zizzo G. Feed-in tariffs for grid-connected PV systems: The situation in the European community. In: Proc. IEEE Conf. on Power Tech, Lausanne, Switzerland; 2007. p. 1981–6.
[5] Hirth L, Ueckerdt F. Redistribution effects of energy and climate policy: The electricity market. Energy Policy 2013;62:934–47.
[6] von Appen J, Braun M, Stetz T, Diwold K, Geibel D. Time in the sun: the challenge of high PV penetration in the German electric grid. IEEE Power Energy Mag 2013;11(2):55–64.
[7] Ogimoto K, Kaizuka I, Ueda Y, Oozeki T. A good fit: Japan's solar power program and prospects for the new power system. IEEE Power Energy Mag 2013;11(2):65–74.
[8] van Werven MJN, Scheepers MJJ. The changing role of distribution system operators in liberalised and decentralising electricity markets. In: Proc. IEEE Int. Conf. on Future Power Systems, Amsterdam, Netherlands; 2005. p. 1–6.
[9] Stetz T, Marten F, Braun M. Improved low voltage grid-integration of photovoltaic systems in Germany. IEEE Trans Sustain. Energy 2013;4(2):534–42.
[10] Tzartzev R, Grady WM, Patel J. Impact of high-penetration PV on distribution feeders. In: Proc. 3rd IEEE PES Int. Conf. and Exhibition on Innovative Smart Grid Technologies (ISGT Europe), Berlin, Germany; 2012. p. 1–6.
[11] Baran ME, Hooshyar H, Shen Zhan, Huang A. Accommodating high PV penetration on distribution feeders. IEEE Trans Smart Grid 2012;3(2):1039–46.
[12] Tonkoski R, Turcotte D, El-Fouly THM. Impact of high PV penetration on voltage profiles in residential neighborhoods. IEEE Trans Sustain. Energy 2012;3(3):518–27.
[13] Masters CL. Voltage rise the big issue when connecting embedded generation to long 11 kV overhead lines. Power Eng J 2002;16(1):5–12.
[14] Katiraei F, Agüero JR. Solar PV integration challenges. IEEE Power Energy Mag 2011;9(3):62–71.
[15] Hill CA, Such MC, Chen Dongmei, Gonzalez J, Grady WM. Battery energy storage for enabling integration of distributed solar power generation. IEEE Trans Smart Grid 2012;3(2):850–7.
[16] Nykamp S, Molderink A, Hurink JL, Smit GJM. Storage operation for peak shaving of distributed PV and wind generation. In: Proc. 2013 IEEE PES Conf. on Innovative Smart Grid Technologies (ISGT'13), Washington, DC; 2013. p. 1–6.
[17] Ueda Yuzuru, Kurokawa K, Tanabe T, Kitamura K, Sugihara H. Analysis results of output power loss due to the grid voltage rise in grid-connected photovoltaic power generation systems. IEEE Trans Ind Electron 2008;55(7):2744–51.
[18] Tonkoski R, Lopes LAC, El-Fouly THM. Coordinated active power curtailment of grid connected PV inverters for overvoltage prevention. IEEE Trans Sustain. Energy 2011;2(2):139–47.
[19] Farhangi H. The path of the smart grid. IEEE Power & Energy Mag 2010;8(1):18–28.
[20] Alam MJE, Muttaqi KM, Sutanto D. Mitigation of rooftop solar PV impacts and evening peak support by managing available capacity of distributed energy storage systems. IEEE Trans Power Syst 2013;28(4):3874–84.
[21] Erol-Kantarci M, Mouftah HT. Wireless sensor networks for cost-efficient residential energy management in the smart grid. IEEE Trans Smart Grid 2011;2(2):314–25.
[22] Corradi O, Ochsenfeld H, Madsen H, Pinson P. Controlling electricity consumption by forecasting its response to varying prices. IEEE Trans Power Syst 2013;28(1):421–9.
[23] Vrettos E, Lai KuanLin, Oldewurtel F, Andersson G. Predictive control of buildings for demand response with dynamic day-ahead and real-time prices. In: Proc. 2013 IEEE European Control Conference, Zürich, Switzerland; 2013. p. 2527–34.
[24] Shao Shengnan, Pipattanasomporn M, Rahman S. Demand response as a load shaping tool in an intelligent grid with electric vehicles. IEEE Trans Smart Grid 2011;2(4):624–31.
[25] Bashash S, Fathy HK. Modeling and control of aggregate air conditioning loads for robust renewable power management. IEEE Trans Control Syst Technol 2013;21(4):1318–27.
[26] Callaway DS, Hiskens IA. Achieving controllability of electric loads. Proc IEEE 2011;99(1):184–99.
[27] Pipattanasomporn M, Kuzlu M, Rahman S. An algorithm for intelligent home energy management and demand response analysis. IEEE Trans Smart Grid 2012;3(4):2166–73.
[28] Bitar EY, Poolla K. Selling wind power in electricity markets: the status today, the opportunities tomorrow. In: Proc. American Control Conference (ACC'12), Montreal, QC; 2012. p. 3144–7.
[29] Ibars C, Navarro M, Giupponi L. Distributed demand management in smart grid with a congestion game. In: Proc. 1st IEEE Int. Conf. on Smart Grid Communications (SmartGridComm'10), Gaithersburg, MD; 2010. p. 495–500.
[30] Mohsenian-Rad A-H, Leon-Garcia A. Optimal residential load control with price prediction in real-time electricity pricing environments. IEEE Trans Smart Grid 2010;1(2):120–33.
[31] Nykamp S, Bosman MGC, Molderink A, Hurink JL, Smit GJM. Value of storage in distribution grids – competition or cooperation of stakeholders? IEEE Trans Smart Grid 2013;4(3):1361–70.
[32] Palensky P, Dietrich D. Demand side management: demand response, intelligent energy systems, and smart loads. IEEE Trans Ind Informatics 2011;7(3):381–8.
[33] Nottrott A, Kleissl J, Washom B. Energy dispatch schedule optimization and cost benefit analysis for grid-connected, photovoltaic-battery storage systems. Renew Energy 2013;55:230–40.
[34] Ru Yu, Kleissl J, Martínez S. Storage size determination for grid-connected photovoltaic systems. IEEE Trans Sustain. Energy 2013;4(1):68–81.
[35] Ru Yu, Kleissl J, Martínez S. Exact sizing of battery capacity for photovoltaic systems. Eur J Control 2014;20(1):24–37.
[36] Riffonneau Y, Bacha S, Barruel F, Ploix S. Optimal power flow management for grid connected PV systems with batteries. IEEE Trans Sustain. Energy 2011;2(3):309–20.
[37] Hubert T, Grijalva S. Modeling for residential electricity optimization in dynamic pricing environments. IEEE Trans Smart Grid 2012;3(4):2224–31.
[38] Darghouth NR, Barbose G, Wiser RH. Customer-economics of residential photovoltaic systems (Part 1): The impact of high renewable energy penetrations on electricity bill savings with net metering. Energy Policy 2014;67:290–300.
[39] Black AJ. Financial payback on California residential solar electric systems. Sol Energy 2004;77(4):381–8.
[40] Sweet B. California's energy-storage mandate. 6th Nov. 2013. Tech. rep., IEEE Spectrum EnergyWise Newsletter.
[41] Candelise C, Winskel M, Gross RJK. The dynamics of solar PV costs and prices as a challenge for technology forecasting. Renew Sustain Energy Rev 2013;26:96–107.
[42] Nair N-KC, Garimella N. Battery energy storage systems: assessment for small-scale renewable energy integration. Energy & Build 2010;42(11):2124–30.
[43] Brown S, Pyke D, Steenhof P. Electric vehicles: the role and importance of standards in an emerging market. Energy Policy 2010;38(7):3797–806.
[44] Ratnam EL, Weller SR, Kellett CM. An optimization-based approach for assessing the benefits of residential battery storage in conjunction with solar PV. In: Proc. IX IEEE Int. Symp. Bulk Power System Dynamics and Control (IREP'13), Rethymno, Greece; 2013. p. 1–8.
[45] Nair NC, Nayagam R, Francis R. New Zealand utility experiences with demand side management. In: Proc. 2008 IEEE Power & Energy Society General Meeting, Pittsburgh, PA; 2008. p. 1–5.
[46] Sedghisigarchi K. Residential solar systems: technology, net-metering, and financial payback. In: Proc. IEEE Conf. on Electrical Power & Energy (EPEC), Montreal, Canada; 2009. p. 1–6.